Kinetics of Polymer Melt Intercalation

Richard A. Vaia, Klaus D. Jandt, Edward J. Kramer,* and Emmanuel P. Giannelis*

Department of Materials Science and Engineering and the Materials Science Center, Cornell University, Ithaca, New York 14853

Received April 7, 1995; Revised Manuscript Received August 15, 1995[⊗]

ABSTRACT: The kinetics of polystyrene melt intercalation in organically modified mica-type silicates were studied using X-ray diffraction and transmission electron microscopy. By monitoring the change in the integrated intensity of the basal reflection of the silicate host, the rate of conversion from unintercalated to intercalated silicate was determined at various temperatures and for various molecular weights of polystyrene. Hybrid formation is limited by mass transport into the primary particles of the host silicate and not specifically by diffusion of the polymer chains within the silicate galleries. The activation energy of hybrid formation is similar to that previously measured for polystyrene self-diffusion in the melt, implying that the mobility of the polymer chains within the host galleries is at least comparable to that in the melt.

Introduction

The intercalation of polymer melts in mica-type layered silicates has recently been reported as a means to synthesize composite materials consisting of alternating nanometer-thick layers of polymer and ceramic.[1,2] The process involves annealing a mixture of polymer and layered silicate powders above the glass transition temperature or melting point of the polymer. During the anneal, the polymer chains diffuse from the bulk polymer melt into the van der Waals galleries between the silicate layers. By judiciously engineering the polymer–silicate interactions, composites have been produced from a broad range of polymers with varying degrees of polarity and crystallinity such as polystyrene, poly(vinylpyridine), poly(ethylene oxide), polysiloxanes, polyphosphazenes, polyamide copolymers, and liquid crystalline copolyesters. As a synthetic approach, polymer melt intercalation is appealing because of its versatility, its compatibility with current polymer processing techniques, and its environmentally benign character due to the absence of solvent. Applications of the resulting polymer–silicate nanocomposite hybrids range from studying polymer chains in a confined environment [3,4] to industrial exploitation of the novel mechanical and electrical properties resulting from the nanometer periodicity of the constituents.[2,5]

To fully explore the potential scientific and industrial applications of polymer melt intercalation, the kinetics of the process must be determined. For example, what is the limiting process involved in hybrid formation? By what mechanism do the chains enter the interlayer? How does the diffusivity of the intercalating chains compare to that of the chains in the bulk? Studies addressing these questions may yield additional insight to the kinetics of chains diffusing into or within confined environments, such as slits or pores. Generally, polymer dynamics in confined environments are a fundamental aspect of many industrially-important fields such as tribology, adhesion, sorption, and catalysis.

Numerous researchers have previously used X-ray and neutron diffraction to study the kinetics of intercalation of small molecules in layered materials.[6–17] The guest species intercalate in the van der Waals gaps between the layers, modifying the lattice structure and altering the scattering behavior of the host. The changes in the scattering profile of the material are a direct result of the intercalation of the guest and, therefore, can be used to monitor the kinetics of the intercalation process.

In this paper, we report on the kinetics of polymer melt intercalation in layered silicates. By monitoring the change in the integrated intensity of the basal reflection of the host, we determined the rate of conversion from unintercalated to intercalated silicate at various temperatures and for various molecular weights of polystyrene. The data are interpreted with regard to the microstructure of the silicate to ascertain the limiting process in hybrid formation. In addition, the implications for hybrid synthesis and the dynamics of polymer chains in confined slits are discussed.

Table 1. Characteristics of Polystyrene

	$\bar{M}_w$	$\bar{M}_w/\bar{M}_n$
PS30	30 000	1.06
PS68	68 000	1.06
PS90	90 000	1.04
PS152	152 000	1.05
Styron 685	300 000	2.6

Experimental Section

Materials. Octadecylammonium-exchanged fluorohectorite (F18) was synthesized from octadecylamine (Aldrich) and Li^+ fluorohectorite (Corning Inc.) by a cation exchange reaction, as outlined previously.[18] Nearly monodispersed polystyrene with characteristics shown in Table I was used as received. Powders of F18 and polystyrene with a narrow particle size distribution were collected using Cu mesh sieves. Claytone 40 (dimethylbis(hydrogenated tallow)ammonium bentonite) was generously donated by Southern Clay Products, Inc. and was used as received. Polystyrene pellets (Styron 685 resin) with characteristics shown in Table I were donated by Dow Chemical Co.

Synthesis. Hybrids were synthesized statically using the following procedure. A 25 mg sample of F18 and 75 mg of polystyrene were mechanically mixed and formed into a pellet using a hydraulic press at a pressure of 70 MPa. Excess polystyrene was used to avoid depletion during intercalation. Polystyrene intercalation was accomplished by annealing the pellet at temperatures greater than the glass transition temperature of polystyrene ($T_g \sim 100$ °C). Samples were formed from polystyrene and F18 powders with the same nominal particle size (175 ± 25 μm). The particle size of F18 was not reduced through the mixing and pressing procedures,

[⊗] Abstract published in *Advance ACS Abstracts,* October 15, 1995.

0024-9297/95/2228-8080$09.00/0

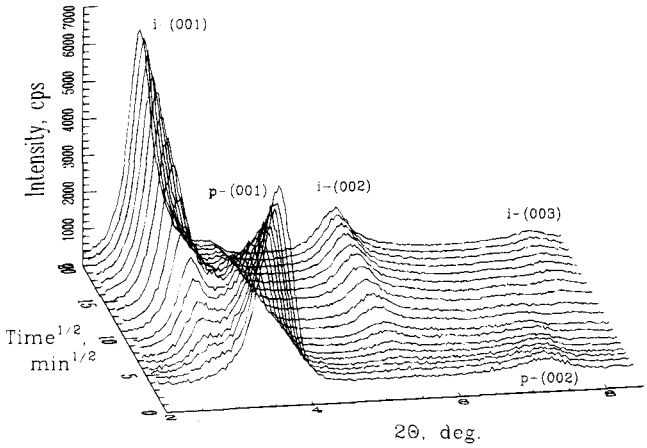

Figure 1. Temporal series of X-ray diffraction patterns for a PS30/F18 pellet annealed in situ at 160 °C in vacuum. Initially, basal reflections from the unintercalated F18, p-(001) and p-(002), are observed at $2\Theta = 4.15$ and $2\Theta = 8.03$, respectively, and correspond to a repeat distance perpendicular to the layers of $d^{p}_{001} = 2.13$ nm. During the anneal, the intensity of the reflections corresponding to the pristine silicate is progressively reduced while a set of new peaks appear corresponding to the PS30/F18 intercalated hybrid. The basal reflections from the intercalated F18, i-(001), i-(002), and i-(003), are observed at $2\Theta = 2.82$, $2\Theta = 5.66$, and $2\Theta = 8.07$, respectively, and correspond to a repeat distance perpendicular to the layers of $d^{i}_{001} = 3.13$ nm.

as indicated by optical and scanning electron microscopy of the samples before annealing. To minimize the effect of variability in constituent mixing, samples used to determine the temperature dependence were formed from a single admixture. Ex-situ kinetic experiments were conducted by periodically removing individual samples from the furnace at specified time intervals. In-situ kinetic experiments were conducted in vacuum on a pellet annealed on a Pt60–Rh40 heating strip in a Buehler temperature-controlled furnace attachment with beryllium windows in a Θ–Θ X-ray diffractometer. Hybrids were also synthesized with a conical screw extruder (Rheocord System 40 Twin Screw Counter Rotating Extruder, Haake-Buchler) at 250 °C using a mechanical mixture of 12.5 g of Clayton 40 and 250 g of Styron 685 resin.

Characterization. X-ray diffraction spectra were collected on a Scintag Inc. Θ–Θ diffractometer equipped with an intrinsic germanium detector system using Cu Kα radiation. Raw diffraction data were corrected using the Lorentz–polarization powder factor and linear background subtraction. To determine the integrated area of the reflections, the diffraction profile was deconvoluted by determining the minimum least squares deviation of the experimental data from a Pearson VII functional form of the diffraction peak.[19] Transmission electron micrographs were taken from 60–100 nm thick, microtomed sections of PS400/F18 hybrids mounted in epoxy using a JEOL 1200 TEM with 120 kV accelerating voltage.

Results and Discussion

Figure 1 shows a temporal series of X-ray diffraction patterns for a 30 000 molecular weight polystyrene (PS30)/F18 mixture annealed in situ at 160 °C in vacuum. The sample contains excess PS30 to avoid polymer depletion during hybrid formation. The X-ray diffraction pattern from the PS30/F18 mixture at the beginning of the anneal contains basal reflections characteristic of the repeat distance of the unintercalated or pristine silicate ($d^{p}_{001} = 2.13$ nm). During the anneal, the intensity of the diffraction peaks corresponding to the pristine silicate is progressively reduced while a set of new peaks appears corresponding to the basal spacing of the PS30/F18 intercalated hybrid ($d^{i}_{001} = 3.13$ nm).

The change in the intensity of the intercalated and pristine diffraction peaks with time reflects the kinetics of the polymer intercalation process. Alexander and Klug have derived the basic relationship between the intensity of an X-ray diffraction peak from a compound to the concentration of that compound in a mixture.[20] The intensity, I_{ij}, of the ith peak of the jth compound in a mixture is given by

$$I_{ij} = \frac{K_{ij} w_j}{\rho_j \mu^*_T} \tag{1}$$

where w_j and ρ_j correspond to the mass fraction and density of compound j, and μ^*_T is the mass absorption coefficient of the mixture. K_{ij} is a constant for a particular reflection and depends on the structure factor for the ij peak and the experimental conditions.[21,22] Since diffraction peaks have a finite width, the integrated intensity, rather than the intensity at the peak angle, best represents I_{ij}.

For reactions involving no mass change and thus constant μ^*_T, the intensity of the reflections from the jth compound is directly proportional to the mass fraction of that compound in the sample, w_j (eq 1). Assuming the number of silicate layers that scatter is conserved during polymer intercalation, the intensities of the pristine and intercalated basal reflections correspond to the concentration of unintercalated and intercalated silicate in the sample. Therefore, the fraction of intercalated silicate, $\chi(t)$, at time, t, may be expressed as

$$\chi(t) = \frac{I_i(t)}{I_i(\infty)} \tag{2}$$

where $I_i(t)$ is the intensity of the intercalated basal reflections at time t and $I_i(\infty)$ is the intensity from a completely intercalated sample. The fraction of unintercalated silicate is $1 - \chi(t)$.

Using eqs 1 and 2, the relative fraction of intercalated silicate may be determined if the intensity of a fully intercalated hybrid is known. In many instances, determining the peak intensity of a fully intercalated hybrid might be too cumbersome. A calibration curve which relates the ratio of the intensities of the pristine to intercalated peaks, $I_p(t)/I_i(t)$, directly to the fraction of silicate intercalated would thus be beneficial. Using eq 1, $I_p(t)/I_i(t)$ may be expressed as

$$\frac{I_p(t)}{I_i(t)} = A^* \frac{1 - \chi(t)}{\chi(t)} \tag{3}$$

where A^* contains the various K_{ij}'s and ρ_j's of the constituents. A^* may be determined from a single series of experiments in which $I_i(\infty)$ is determined for a given mixture of constituents. Once A^* is known, eq 3 may then be used to determine the fraction of silicate intercalated from the ratios of pristine to intercalated peak intensities for samples with the same composition, constituent mixing, and diffraction geometry used to determine A^*.[23] From a series of in-situ experiments conducted to completion, an average value of $A^* = 1.2$ for PS30/F18 was obtained.

Using the methodology discussed above, the fraction of intercalated silicate for various times, temperatures, and molecular weights was determined from the X-ray diffraction patterns. Figure 2 shows the fraction of intercalated silicate as a function of time at various temperatures for PS30. At 170 and 180 °C, the samples

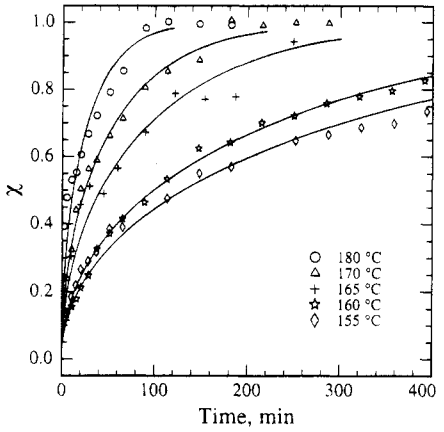

Figure 2. Fraction of F18 intercalated as the anneal progresses at 155, 160, 165, 170, and 180 °C for PS30. Solid lines are best fits to the data using eq 4.

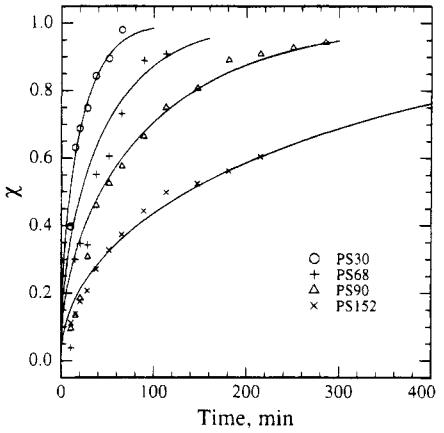

Figure 3. Fraction of F18 intercalated as the anneal progresses at 180 °C for PS30, PS68, PS90, and PS152. Solid lines are best fits to the data using eq 4.

were annealed until complete intercalation occurred, whereas at 155, 160, and 165 °C, the data were obtained using $A^* = 1.2$. All data were collected in situ with the exception of the anneal at 165 °C which was collected ex situ. Figure 3 shows the fraction of intercalated silicate as a function of time at 180 °C for various molecular weights of polystyrene. For PS30 and PS90, the samples were annealed until complete intercalation occurred, whereas for PS68 and PS152, the data were obtained using $A^* = 1.2$. All data were collected in situ.

The conversion of a pristine organosilicate to an intercalated hybrid requires polymer chains to be transported from the molten bulk into the silicate interlayer. Therefore, the morphology of the F18 particle must be known to analyze the kinetic data. Figure 4 summarizes the morphology of the silicate particles. The silicate particles which are mixed with the polystyrene powder are nominally 175 μm in diameter. Transmission electron images of partially annealed samples indicate that these particles are composed of an agglomeration of smaller, oblong-shaped particles. We will refer to the large silicate particles as *agglomerates* and the oblong particles as *primary particles*. From TEM, we find that the size of the agglomerate is related to the size of these primary particles—larger agglomerates are nominally composed of larger primary particles. The primary particles generally have aspect ratios from 2 to 10 with a major axis dimension from a few tenths to ten microns.

The primary particles generally consist of a compact face-to-face stacking or low-angle intergrowth of individual silicate *crystallites* (tactoids). A TEM bright field image of a representative region of the polystyrene–F18 hybrid showing a primary particle (dark central feature) surrounded by a matrix of polystyrene is displayed in Figure 5a. The crystallites are visible as regions of alternating narrow, dark, and light bands within the primary particle. They are tightly packed and generally are oriented along the major axis of the primary particle. TEM images reveal that the size of the crystallites are independent of the size of the primary particles. As seen in Figure 5b, the individual crystallites consist of stacks containing between 10 and 100 parallel, equally spaced aluminosilicate layers (dark bands). The layers are roughly circular, 0.05–0.5 μm in diameter, and ~10 Å thick. They are separated by a van der Waals interlayer or gallery (light bands), which contains octadecylammonium cations (~10 Å thick) in the pristine organosilicate. The organic cations render the hydrophobic silicate surface organophilic. The morphology of the F18 particles is similar to that of bentonites and vermiculites.[24-26]

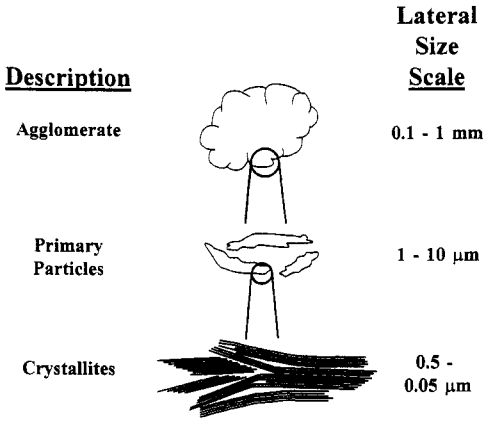

Figure 4. Schematic of the morphology of the F18 particles.

The increased basal spacing associated with hybrid formation arises from the expansion of the gallery perpendicular to the silicate layers to accommodate the intercalated polymer. Generally, the accessibility of the interlayer to the polymer chains depends on the location of the primary particle within the agglomerate and the location and orientation of the crystallites within the primary particle. Crystallites near the edge will be more accessible to the polymer chains than those near the center. Since the silicate layers are impenetrable, the polymer must enter the gallery from the edges of the crystallites. Therefore, for intercalation to occur, polymer must be transported from the agglomerate/polymer melt interface to the primary particles and then to the edges of the crystallites. The TEM micrographs indicate that for the agglomerate sizes used in this study, the polymer penetrates the agglomerate and surrounds the individual primary particles before substantial hybrid formation occurs. Therefore, we assume penetration of the agglomerate is not a limiting step for hybrid formation and each primary particle is essentially surrounded by the polymer melt.

Thus, hybrid formation may be thought of as occurring one of two ways, depending on the path of polymer transport into the primary particle. If mass transport *through* the crystallites (i.e. within the silicate galleries) is much slower than *between* the crystallites (i.e. via the intercrystallite volume), individual crystallites will be surrounded by polymer, independent of their location within the primary particle. Thus, at a given time, all

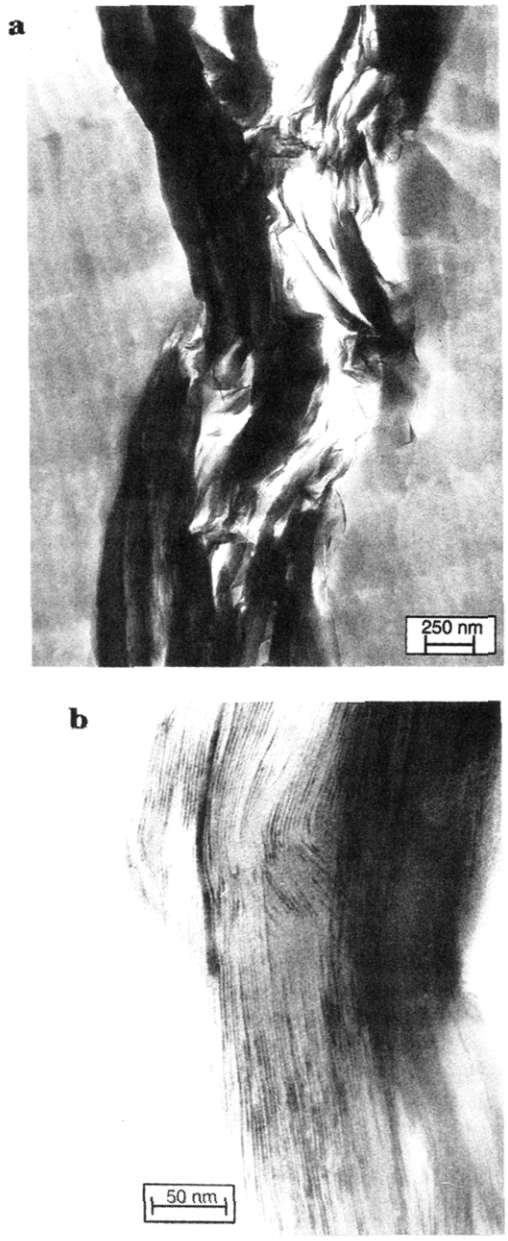

Figure 5. (a) Bright field TEM micrograph of the F18 primary particle, dark central feature, surrounded by a matrix of polystyrene. (b) Bright field TEM micrograph of a silicate crystallite found within the primary particle. The coherent stacking of the silicate layer and interlayer are visible as regions of alternating narrow, dark, and light bands (lattice fringes).

the crystallites in the primary particle would be intercalated to the same extent. In this case, the kinetics of hybrid formation would be independent of the size of the primary particles. Alternatively, if mass transport through the crystallites is comparable to that between the crystallites, polymer will penetrate from the outside of the primary particle as a front, leaving behind completely intercalated crystallites. Crystallites on the interior side of the front would be unintercalated. In this case, the kinetics of hybrid formation would depend on the gross size of the primary particle.

Figure 6 compares hybrid formation from two F18 powders with agglomerates nominally greater than 200 μm and less than 100 μm, respectively. Recall that the mean size of the primary particle scales with the size of the agglomerate. After 40 min at 170 °C, polymer intercalation in the mixture containing smaller primary

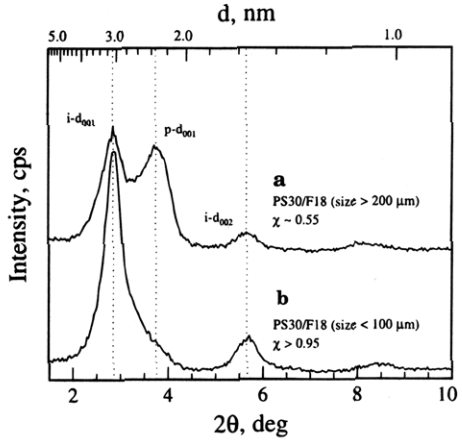

Figure 6. X-ray diffraction patterns from PS30/F18 pellets with different F18 agglomerate sizes [(a) agglomerates nominally greater than 200 μm and (b) agglomerates nominally less than 100 μm] annealed for 40 min at 170 °C.

particles is almost complete whereas intercalation into the mixture containing larger primary particles is only 55% complete. The dependence of polymer intercalation on gross agglomerate size indicates the hybrid formation occurs by mass transport of the polymer melt into the primary particle.

In accordance with these results, consider that mass flow into the primary particle and subsequent hybrid formation may be described as a Fickian process with a single, apparent diffusivity.[27] Since the crystallites are preferentially aligned along the primary particle major axis, mass flow is inhibited along the minor axis of the primary particle because of the impenetrability of the aluminosilicate layers. Therefore, polymer diffusion into the primary particle may be modeled as mass flow through the curved lateral surface of a cylinder with impermeable flat circular faces of area equal to the mean primary particle size. Initially, the concentration at the lateral surface of the primary particle is zero and for $t > 0$, the concentration is constant. Assuming the apparent diffusivity, D, is concentration independent, the ratio of the amount of polymer intercalated, $Q(t)$, to that at equilibrium, $Q(\infty)$ is[28,29]

$$\frac{Q(t)}{Q(\infty)} = 1 - \sum_{m=1}^{\infty} \frac{4}{\alpha_m} \exp\left(-\frac{D}{\bar{a}^2}\alpha_m t\right) \qquad (4)$$

where $D/\bar{a}^2$ is the effective diffusional rate, $\bar{a}$ is the mean radius of the flat impermeable surface of the primary particle, and α_m is the mth positive root of the Bessel function of zeroth order, $J_0(a) = 0$. Since the fraction of silicate intercalated corresponds to the amount of intercalated polymer, the fraction of intercalated silicate, χ, equals $Q(t)/Q(\infty)$. The experimental data in Figures 2 and 3 were fit using eq 4 with the effective diffusional rate, $D/\bar{a}^2$, as the only adjustable parameter.[30]

Assuming the effective diffusional rate has an Arrhenius temperature dependence, the activation energy of melt intercalation of PS30 in F18 is approximately 166 ± 12 kJ/mol. The activation energy is comparable to the activation energies measured for self-diffusion of polystyrene (167 kJ/mol[33–35]) at similar temperatures and with similar molecular weights.[27] The agreement between the activation energies suggests that the largest energy barrier to hybrid formation is comparable to that of chain motion in the polymer melt. Additionally,

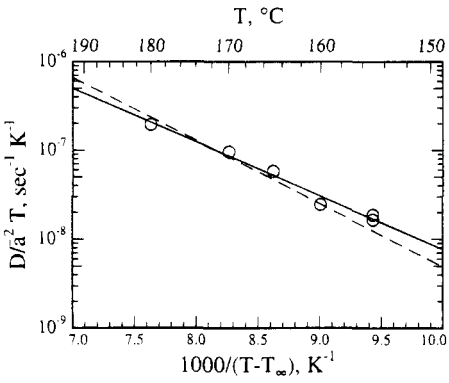

Figure 7. Comparison between the effective diffusional rates, $D/\bar{a}^2$, for PS30 melt intercalation in F18 and the Vogel equation (dashed line) using empirical parameters from the literature which were obtained by fitting the η_0 for polystyrene (B = 710 K and T_∞ = 49 °C).[33,36] The least squares fit of the data (solid line) yields B = 604 ± 40 K.

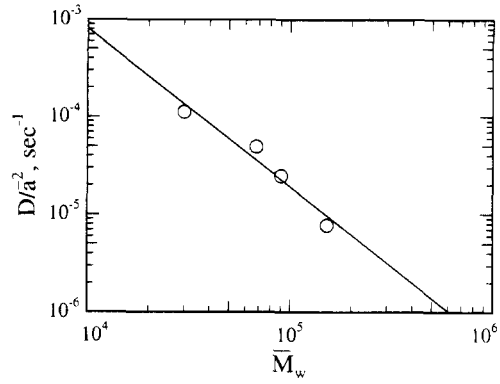

Figure 8. Effective diffusional rate, $D/\bar{a}^2$, for melt intercalation of PS30, PS68, PS90, and PS152 in F18. The least squares fit of the data (solid line) yields a slope of −1.6.

the apparent diffusivities, D, determined from the effective diffusional rates, assuming that $\bar{a}$ is approximately 5 μm, as determined by TEM, are the same order of magnitude (10^{-11} cm^2/s at 170 °C) as self-diffusion coefficients of polystyrene determined at comparable temperatures and molecular weights.[33-35] Since the rate of hybrid formation is comparable to polymer self-diffusion in the bulk, the confinement of the polymer within the silicate galleries as a result of intercalation does not inhibit chain motion.

Because of the apparent link between the rate of hybrid formation and polymer self-diffusion, the temperature dependence of hybrid formation should be describable by the Vogel equation (or the equivalent WLF equation) for polystyrene tracer diffusion in the melt, $\log(D^*/T) = A' - B/(T - T_\infty)$.[33] Figure 7 compares the effective diffusional rates from the experiments summarized in Figure 2 to the Vogel equation (dashed line) using empirical parameters from the literature (B = 710 K and T_∞ = 49 °C, obtained from the zero-shear rate viscosity, η_0, of polystyrene).[33,36] The least squares fit (solid line) yields B = 604 ± 40 K. The qualitative agreement between the Vogel relationship and the experimental data is reasonably good. Differences may be attributed to the assumption that T_∞ for the intercalating polymer is the same as for the polymer in the melt. The intermolecular environment of the intercalated polymer is considerably different from that in the melt. Therefore, the monomeric friction coefficient, and thus T_∞, of the intercalated polymer should also differ from that in the bulk melt. Previous work indicating that the intercalated polystyrene exhibits a marked suppression or absence of a bulk glass transition, as judged by differential scanning calorimetry, supports this contention.[1]

As demonstrated in Figure 3, the kinetics of hybrid formation should also depend strongly on the molecular weight of the polymer. Figure 8 shows $\log(D/\bar{a}^2)$ versus $\log(\bar{M}_w)$ from the experiments summarized in Figure 3. A least square fit to the data gives a slope of −1.6 over our limited molecular weight range; however there is some evidence of a steeper power law dependence at the higher $\bar{M}_w$'s. Since the contour length of the polymer chains is less than the size of the primary particles or the crystallites, polymer motion within the primary particle is essentially two-dimensional, confined to the silicate galleries or to the small volume between the crystallites. There is thus no reason to expect the molecular weight dependence of $D/\bar{a}^2$ for polymer intercalation to be the same as that for self-diffusion in the bulk, i.e. $D \sim M_W^{-2}$.[35] Nevertheless, the slope of our data for the three highest molecular weights is close to −2. However, it seems unlikely that the "tube" model,[37] which describes the reptation of polymers in the bulk, can be used to rationalize the diffusion of polymers in the two-dimensional galleries between the aluminosilicate layers. Additional experimental investigations and a detailed theoretical development is necessary to explain the observed molecular weight dependence of hybrid formation.[27]

Since mass transport into the primary particle is the limiting step to hybrid formation, the degree of constituent mixing is critical for rapid hybrid formation. Dynamic mixing during the anneal, in an extruder for example, will decrease the hybrid formation time by breaking up primary particles and increasing sample uniformity. Our static experiments thus represent an upper bound for the hybrid formation time under such mixing conditions. Extrapolating the kinetics determined from polystyrene–F18 to conventional polystyrene processing temperatures (250 °C) indicates full hybrid formation should require about 10 min for polystyrene of $\bar{M}_w$ = 300 000, typical for commercial polymers (see Table 1). Experiments conducted in an extruder at 250 °C with Styron 685 pellets and Claytone 40 indicate that the resident time (~4 min) in the extruder was more than sufficient to achieve full hybrid formation.

Conclusion

Polystyrene melt intercalation in organically modified mica-type silicates occurs by mass transport into the primary particles of the silicate and is not specifically limited by diffusion of the polymer chain within the silicate gallery. The activation energy of hybrid formation is similar to that previously measured for polystyrene self-diffusion in the bulk melt, implying that the mobility of the polymer chains within the interlayer space of the silicate is comparable to that in the bulk. Therefore, hybrid formation requires no additional processing time than currently required by conventional polymer processing techniques such as extrusion.

Acknowledgment. Primary support of this work came from the Materials Science Center (MSC) at Cornell University (funded by NSF-DMR-MRSEC) and its Polymer Outreach Program through grants from Corning, Inc. and from generous gifts by DuPont, Xerox, and Southern Clay Products. R.A.V. gratefully acknowledges the financial support of a DoD National Defense

Science and Engineering Fellowship. K.D.J. gratefully acknowledges partial financial support from the Feodor-Lynen-Fellowship of the Alexander von Humboldt Foundation, Bonn, Germany. We thank C. Smith and E. Fewkes, Corning Inc., for use of the extruder and C. Daugherty, N. Rizzo, J. Hunt, and I. Karr for their assistance. This study benefited from the use of the Central Facilities of the MSC.

References and Notes

(1) Vaia, R. A.; Ishii, H.; Giannelis, E. P. *Chem. Mater.* **1993**, *5*, 1694.
(2) Vaia, R. A.; Vasudevan, S.; Krawiec, W.; Scanlon, L. G.; Giannelis, E. P. *Adv. Mater.* **1995**, *7*, 154.
(3) Vaia, R. A.; Sauer, B. B.; Tse, O.; Giannelis, E. P.; Mehrotra, V. Submitted for publication to *J. Polym. Sci., Part B: Polym. Phys.*
(4) Wong, S.; Vasudevan, S.; Vaia, R. A.; Giannelis, E. P.; Zax, D. *J. Am. Chem. Soc.*, in press
(5) Krawiec, W.; Scanlon, L. G.; Fellner, J. P.; Vaia, R. A.; Vasudevan, S.; Giannelis, E. P. *J. Power Sources*, in press.
(6) McAtee, J. L.; Hawthorne, J. W. *Am. Mineral.* **1964**, *49*, 247.
(7) Adams, J. M.; Thomas, J. M.; Walters, M. J. *J. Chem. Soc., Dalton Trans.*, **1975**, 1459.
(8) Acrivos, J. V.; Dellus, C.; Topsøe, N. Y.; Salem, J. R. *J. Phys. Chem.* **1975**, *79*, 3003.
(9) Breen, C.; Adams, J. M.; Riekel, C. *Clays Clay Miner.* **1985**, *33*, 275.
(10) Evans, J. S. O.; O'Hare, D. *Adv. Mater.* **1994**, *6*, 646.
(11) Adams, J. M.; Breen, C. *J. Colloid Interface Sci.* **1982**, *89*, 272.
(12) Slabaugh, W. H.; Hiltner, P. A. *J. Phys. Chem.* **1968**, *72*, 4295.
(13) Solin, S. A. In *Intercalation in Layered Solids*; Dresselhaus, M. S., Ed.; NATO ASI Series B, Phys. Vol. 148; Plenum Press: New York, 1986; pp 173–183.
(14) Riekel, C.; Schollhorn, R. *Mater. Res. Bull.* **1976**, *11*, 369.
(15) Cebula, D. J.; Thomas, R. K.; White, J. W. *Clay Clay Miner.* **1981**, *29*, 241.
(16) Ross, D. K.; Hall, P. L. In *Advanced Chemical Methods for Soil and Clay Minerals Research*; Stucki, J. W., Banwort, W. L., Eds.; D. Riedel: Dordrecht, Holland; 1980; pp 93–168.
(17) Rao, G. V. S.; Shafer, M. W. In *Intercalated Layered Materials*; Lévy, F., Ed.; D. Reidel: Dordrecht, Holland, 1979; pp 99–199.
(18) Vaia, R. A.; Teukolsky, R. K.; Giannelis, E. P. *Chem. Mater.* **1994**, *6*, 1017.
(19) Brown, A.; Linde, S. *Adv. X-ray Anal.* **1986**, *30*, 343.
(20) Klug, H. P.; Alexander, L. E. *X-ray Diffraction Procedures*, 2ed.; John Wiley and Sons: New York, 1974; pp 365–368, 549–553.
(21) Synder, R. L.; Bish D. L. In *Modern X-ray Diffraction*; Bish, D. L., Post J. E., Eds.; Reviews in Mineralogy Vol. 20; Mineralogical Society of America: Washington, DC, 1989; pp 101–144.
(22) Epple, M.; Cammenga, H. K., *Ber. Bunsen-Ges. Phys. Chem.* **1992**, *96*, 1774.
(23) Scattering theory implies A^* is temperature dependent, and therefore special care must be taken when assuming it to be constant over a large temperature range. Over the temperature range examined in this work, the integrated intensity of the (001) silicate reflection was experimentally found to change less than 5%.
(24) Grim, R. E.; Güven, N. *Bentonites: Geology, Mineralogy, Properties and Uses*; Elsevier: New York, 1978; pp 13–23.
(25) Güven, N. In *Hydrous Phyllosilicates*,; Bailey, S. W., Ed.; Reviews in Mineralogy Vol. 19; Mineralogical Society of America: Washington, DC, 1988; pp 497–560.
(26) Vali, H.; Hesse, R.; Kohler, E. E. *Am. Mineral.* **1991**, *76*, **1973**.
(27) Polystyrene penetration of the primary particle may also be considered to be driven by capillary forces associated with the creation of a new particle/polymer interfacial area. As penetration proceeds, the distance over which the capillary pressure drops increases and the pressure gradient causing the flow decreases in such a way that on the basis of the time dependence of intercalation alone, a capillary pressure driven permeation cannot be distinguished from diffusion. Similarly, because the temperature dependence of diffusion and viscosity depend primarily upon the temperature dependence of the monomer friction coefficient, the mechanism is not discernible on the basis of the temperature dependence of intercalation (Figure 7). It may be possible to distinguish the mechanisms on the basis of examining the molecular weight dependence of hybrid formation over a larger range of molecular weights than heretofore possible (Figure 8). Such studies are underway.
(28) Barrer, R. M.; Craven, R. J. B. *J. Chem. Soc., Faraday Trans.* **1992**, *88*, 645.
(29) Breen, C.; Deane, T.; Flynn, J. J.; Reynolds, D. *Clays Clay Miner.* **1987**, *35*, 336.
(30) Hybrid formation may also be described by Fickian diffusion into a sphere or by the propagation of a constant concentration front into a sphere.[10,31,32] The elongated nature of the primary particles may be taken into account by assuming the volume of the model sphere is equal to the average volume of the primary particle. The agreement with experimental data and the activation energy of the process is the same as determined from the cylindrical model. The difference between the approaches arises in the relationship between the effective diffusional rate and the diffusivity. The cylindrical model was chosen because it best describes the morphology of the primary particles.
(31) Timofeev, D. P. *Adv. Chem.* **1971**, *102*, 247.
(32) Kärger, J.; Ruthven, D. M. *Diffusion in Zeolites and other Microporous Solids*; John Wiley and Sons: New York, 1992; pp 250–255.
(33) Green, P. F.; Kramer, E. J. *J. Mater. Res.* **1986**, *1*, 202.
(34) Antonietti, M.; Coutandin, J.; Grütter, R.; Sillescu, R. H. *Macromolecules* **1984**, *17*, 798.
(35) Tirrell, M. *Rubber Chem. Technol.* **1984**, *57*, 523.
(36) Graessley, W. W.; Roovers, J. *Macromolecules* **1979**, *12*, 959.
(37) Doi, M; Edwards, S. F. *Theory of Polymer Dynamics*; Oxford University Press: Oxford, U.K., 1986.

MA950482C